# Performance comparison of external IBA and SR-XRF imaging for the study of ivory

Laurent Tranchant, Katharina Müller, Quentin Lemasson, Laurent Pichon, Sebastian Schöder, Nicholas John Conard, Ina Reiche

Nuclear Instruments and Methods in Physics Research B 545 (2023) 165146

Contents lists available at ScienceDirect

Nuclear Inst. and Methods in Physics Research, B

journal homepage: www.elsevier.com/locate/nimb

Full Length Article

# Performance comparison of external IBA and SR-XRF imaging for the study of ivory

L. Tranchant [a,b], K. Müller [b], Q. Lemasson [c,d], L. Pichon [c,d], S. Schöder [a], N.J. Conard [e,f], I. Reiche [d,g,*]

[a] Synchrotron SOLEIL, BP 48 Saint-Aubin, 91192 Gif-sur-Yvette, France
[b] IPANEMA, CNRS, Ministère de la culture, UVSQ, MNHN, UAR 3461, Université Paris Saclay, 91192 Gif-sur-Yvette, France
[c] Centre de recherche et de restauration des musées de France, C2RMF, Palais du Louvre, 75001 Paris, France
[d] Fédération de recherche NewAGLAE, FR3506 CNRS/Ministère de la Culture/ChimieParistech – PSL, Palais du Louvre, 75001 Paris, France
[e] Abt. Altere Urgeschichte und Quartärökologie, Uni Tübingen, Burgsteige 11, 72070 Tübingen, Germany
[f] Senckenberg Centre for Human Evolution and Paleoenvironment, Schloss Hohentübingen, University of Tübingen, 72010 Tübingen, Germany
[g] PSL Université, ENSCP, Institut de recherche de Chimie Paris, UMR 8247 CNRS, Equipe PCMTH, 75005 Paris, France

ARTICLE INFO

*Keywords:*
Mammoth ivory
Prehistoric objects
PIXE
PIGE
RBS
Synchrotron radiation XRF

ABSTRACT

The performances of Ion Beam Analysis (IBA) at the New AGLAE accelerator external microfocus beamline and those of Synchrotron Radiation micro-X-Ray Fluorescence (SR-XRF) at the PUMA beamline at the SOLEIL synchrotron are compared for non-invasive characterization of archaeological ivory. Based on the examination of ivory artefacts from the Palaeolithic site *Hohle Fels* in South-western Germany, the informative value of this combination of methods is evaluated with regard to archaeological questions. Parameters such as depth of information, elemental sensitivity as a function of atomic number and imaging capacity are considered. We obtain an almost complete coverage of the chemical composition of ivory (C to Pb). Rutherford Backscattering Spectrometry (RBS) allows the identification of collagen and PIXE/PIGE provide a higher sensitivity for light elements while SR-XRF offers high resolution imaging for heavier elements. Both facilities provide different depths of information that can be exploited to better distinguish exogenous and endogenous elements.

## 1. Introduction

Mammoth ivory objects can be considered as an archive of ways of life in prehistoric societies in the absence of written sources. Ivory coming from the tusks of elephants and mammoths is a biomineral that registers in its chemical and isotopic composition geochemical proxies indicative of diets, climatic conditions and the environment in which the animal lived [1,2]. Transformed into tools and symbolic objects studying the ivory material can also bring to light information about the use and the meaning of such objects in prehistoric times [3,4]. Body ornaments and sculptures made of mammoth ivory belong to the first art objects of our human history. Therefore, these objects are important witnesses studied in archaeological sciences.

Ivory is a hierarchically bio-composite material consisting of a mineral phase (carbonated hydroxyapatite (carb-HAP, $Ca_{10}(PO_4)_6OH_2$ rich in Mg, about 70 wt%), an organic phase (mainly collagen type I, about 20 wt%) and water (10 %) [5,6]. In the course of time, the chemical composition of major, minor and trace elements of ivory may change heterogeneously due to taphonomical processes. On the one hand, the above-mentioned geochemical markers, which are based on the endogenous ivory composition, might have changed, on the other hand, exogenous elements might have enriched in ivory. As a result, a wide variety of minor and trace elements from fluorine to lead is present in ancient ivory [7,6].

Because of the precious nature of ancient mammoth ivory objects, analyses of their chemical composition must be performed preferentially non-invasively and without sampling. To date, few analytical studies have been conducted on ancient ivory [7,8,6,9]. Chemical analyses by Particle Induced X-ray and gamma ray emission (PIXE/PIGE) or X-ray fluorescence analysis (XRF) are well suited for the study of ivory artifacts, as they allow non-destructive and simultaneous examination of a broad range of chemical elements with high sensitivity and micro-scale

* Corresponding author at: Fédération de recherche NewAGLAE, FR3506 CNRS/Ministère de la Culture/ChimieParistech – PSL, Palais du Louvre, 75001 Paris, France.
*E-mail address:* ina.reiche@chimieparistech.psl.eu (I. Reiche).

https://doi.org/10.1016/j.nimb.2023.165146
Received 31 May 2023; Received in revised form 19 October 2023; Accepted 23 October 2023
Available online 4 November 2023

resolution [10,11]. PIXE/PIGE can additionally be combined with Rutherford Backscattering Spectrometry (RBS) allowing the analysis of light elements such as C and N [12]. X-ray fluorescence performed at synchrotron sources even allows for improving the detection limits of a large range of elements. New analytical development of PIXE and of synchrotron radiation XRF (SR-XRF) allows for performing analyses under atmospheric pressure (air or He atmosphere) in imaging mode [13,14,15].

Our previous research on Palaeolithic mammoth ivories using external combined micro-PIXE/PIGE showed specific chemical differences as a function of the state of preservation and origin of the artifacts. It was shown that certain trace and minor elements such as Fe and Mn enrich in mammoth ivory during diagenetic processes whereas Mg is lost over time [6,16]. Furthermore, elements like Zn, Sr and Br seem to be biogenic trace elements in mammoth ivory that can be used as a tracer of ivory origin. Thus, regional differences in the ivory procurement strategies could be discussed this way [7,9]. Endogenous elements usually show a homogeneous distribution along the cross-section with slight variations due to changes in environmental conditions during the lifetime of the individual, whereas exogenous elements, with a few exceptions, show a heterogeneous distribution along the cross-section with elevated values near the outside of the sample [7].

However, previous studies with microPIXE/PIGE were based on point analyses, i.e., averages over the studied area were considered and the heterogeneity of the material was not fully taken into account. In this study, 2D mappings were performed by microPIXE/PIGE/RBS and SR-XRF to investigate elemental distributions in ivory and bone with high spatial resolution and high sensitivity. The utility of imaging techniques is particularly advantageous for the study of diagenetic changes, as these are usually leading to heterogeneous elemental distributions in the material. Here, the performances of these imaging techniques are compared, their strengths and limitations are elaborated with respect to the analysis of prehistoric ivory considering also different information depths of the techniques.

The combined microPIXE/PIGE analyses allow for the detection of main, minor and trace elements between F and Pb, providing a good description of the elemental composition of the mineral phase of ivory. Lighter elements such as C and N, which are characteristics of the organic phase of ivory (collagen), have not been considered so far for mammoth ivory [10].

In this paper, the optimization of the analytical approach for the study of light elements is presented by combining external microPIXE/PIGE with external RBS analyses. Particularly, information on the preservation of collagen in ancient ivory can potentially be obtained. Finally, the complementarity of the applied SR-XRF and ion beam analyses (IBA) analytical methods is discussed for a non-invasive, quasi-total chemical characterization of ancient ivory artefacts, generally presenting less collagen than modern ivory. It is consistent to compare two large scale facilities for their performances with respect to the study of prehistoric ivory artefact because in both cases the artefacts need to be transported to the analytical facility.

## 2. Material and methods

### 2.1. Studied material

The archaeological material considered in this study come from the Hohle Fels cave, a prehistoric site located in Southwest of Germany. This site is of great importance to prehistorians because the earliest example of expressly human figurative art (female figurine from Hohle Fels) and some of the oldest musical instruments ever found have been discovered there [3,17]. Moreover, Hohle Fels cave has been occupied successively by *Homo sapiens neanderthalensis* and then by *Homo sapiens sapiens*.

A total of twelve archaeological ivory and ten bone samples from the Hohle Fels, dated to the Aurignacian (ca. 30,000 to 40,000 years ago), have been analyzed as part of a long-standing research study on Paleolithic ivory and are published elsewhere with emphasis on taphonomic conclusions [11]. In this paper, we present results for two of these archaeological ivory samples from Hohle Fels (AI-HF-03 and AI-HF-06, Fig. 1), which were selected because they are particularly useful for discussing methodological issues and highlighting the advantages of combining IBA and SR-XRF analyses with respect to the study of ancient ivory. The sample AI-HF-03 allows a straightforward comparison between mappings obtained at New AGLAE and at PUMA and sample AI-HF-06 is one of the few samples with a large amount of carbon detected on the chosen analyzed area, allowing RBS mapping. All the ivory samples studied in this paper are unworked ivory fragments, they have not been cut or polished after excavations.

### 2.2. Experimental

The accelerator AGLAE was used for the chemical characterization of ancient ivory artefacts by IBA. The experimental imaging setup of the New AGLAE external microfocus beamline is presented in Fig. 2a. 3 MeV protons are focused to a microbeam and extracted on the sample placed at 2 mm in the front of the beamline with an $Si_3N_4$ exit window under He atmosphere [14]. The external beam set-up is equipped with four silicon drift detectors (SDD) for the detection of X-ray (PIXE), a charged particle detector for RBS, a HPGe $\gamma$-detector for PIGE and a microscope for sample positioning. PIXE, PIGE and RBS analyses were performed simultaneously under He flow and atmospheric pressure in imaging mode [18,19,20].

Synchrotron radiation XRF measurements were performed at the PUMA beamline of the SOLEIL synchrotron, which is dedicated to X-ray based studies in the field of cultural heritage research. The experimental setup of PUMA is presented in Fig. 2b. The energy of the X-ray beam is tunable between 4 and 22 keV using a Si(1 1 1) fixed exit double-crystal monochromator. A Kirkpatrick-Baez (KB) mirror allows the beam to be focused to a spot size of a few micrometers. The samples are arranged in a 45°/45° geometry with respect to the incident beam and the X-ray fluorescence detector (SDD). A video-microscope is pointed perpendicular to the sample surface. For SR-XRF mapping, an incident beam energy of 18 keV was used because this energy allows to induce K-shell or L-shell emissions for every element between P and U that can be detected in ivory [13,21].

The measuring conditions were optimized to make the PIXE and SR-XRF mappings qualitatively comparable. As far as possible, on each sample the same area was analyzed at both facilities (maximal 1.5 × 1.5 $mm^2$). The intensity of the beam flux was about $1.5 \times 10^{10}$ photons/s for an acquisition time of 0.5 s per pixel at PUMA and $3.6 \times 10^{10}$ protons/s for a total charge of 9.7 μC at New AGLAE. Synchrotron radiation XRF mapping was realized with a beam spot size of 10 μm × 5 μm and a step size of 10 μm. The size of the proton beam for PIXE/PIGE/RBS mappings was about 40 μm × 40 μm and the step size was 10 μm. The other measurement conditions were the same for PIXE/PIGE/RBS mappings. The acquisition time was adapted to obtain a good trade-off between high statistics and low irradiation time to minimize possible damage of the samples. The total duration of a mapping was approximately 39 min at PUMA and 28 min at New AGLAE.

### 2.3. Data evaluation and mapping representation mode

The RBS spectra have been fitted with the software SIMNRA [22]. The cross sections of some target elements ($Z < 30$) are non-Rutherford for a 3 MeV proton incident beam. However, non-Rutherford cross sections of Al, Ca and P at 135° (corresponding to the scattering angle $\theta$ between the backscattered exit beam and the surface normal to the sample [22]) provide a non-optimal fitting of the experimental data (see the Fig. 3b and S5 in the supplementary information (SI)). Therefore, Rutherford cross sections were used for Al, P, Ca and Mn in the RBS fits. Even though this approximation is incorrect at these energies [22], the resulting fit appears to be correct. The reason for this is still unclear and


**Fig. 1.** Photographs of the ivory samples AI-HF-03 (a) and AI-HF-06 (b) from Hohle Fels cave. The analyzed area is located in the area marked with a red circle for AI-HF-03 and presented at the extremity of the red arrow for AI-HF-06.

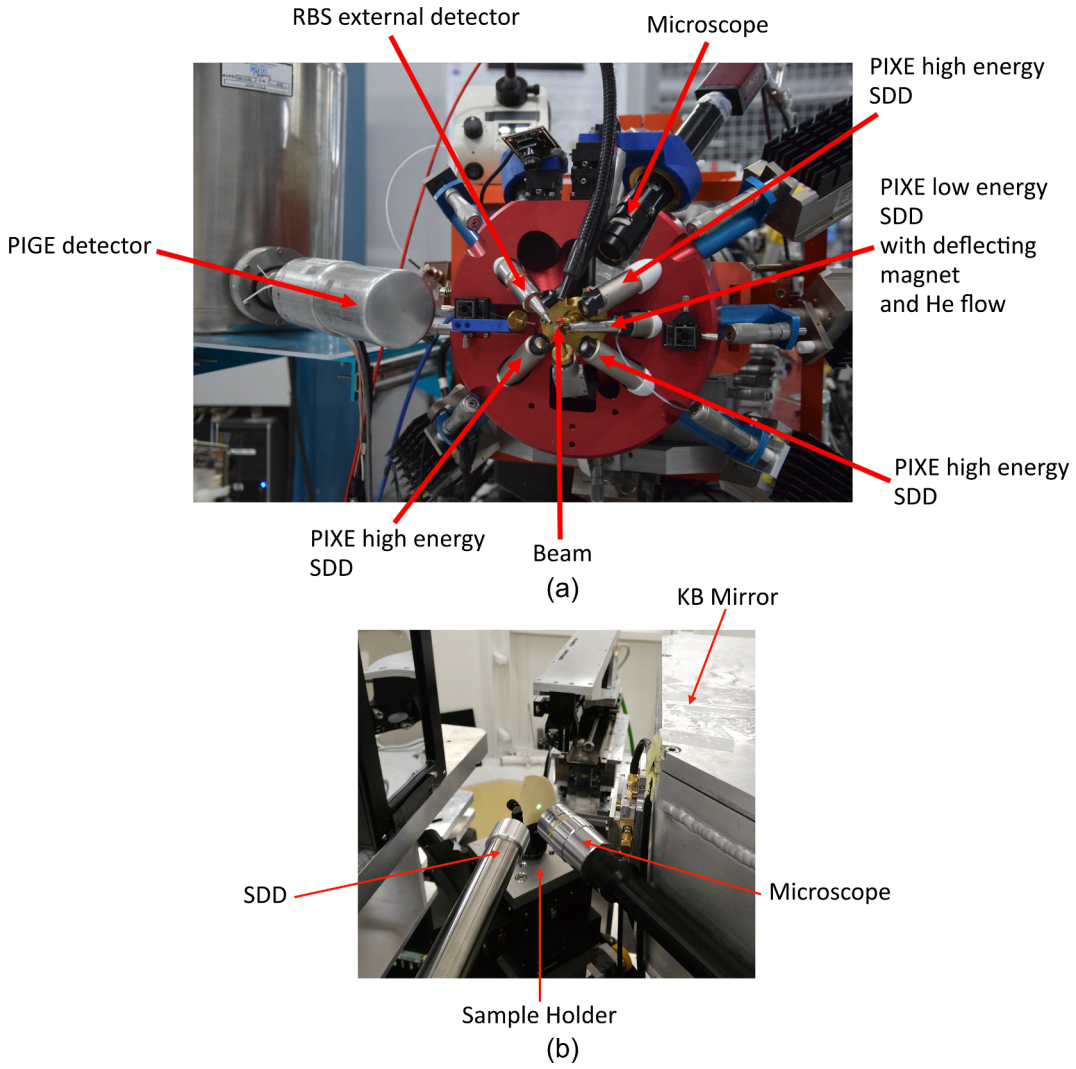


**Fig. 2.** Upper part: (a) Experimental imaging setup of New AGLAE. Lower part: (b) Experimental imaging setup of the PUMA beamline with a sample of elephant ivory.

is beyond the scope of this study.

The RBS C map data in the Fig. 4b were obtained by subtracting a region of interest (ROI) in the sum spectrum around 2000 keV containing the contributions of backscattered protons by C, O and Ca (ROI $\alpha$ in the Fig. 4c) by a ROI around 2300 keV corresponding to the contributions of O and Ca (ROI $\beta$ in the Fig. 4c) to the RBS signal [23]. Both ROIs $\alpha$ and $\beta$ have the same energy width (about 50 keV). A median filter with 3 pixels width has been used to mitigate the noise of RBS mappings and we replaced negative values resulting from the subtraction by zero.

PIXE, PIGE and SR-XRF mappings were processed using PyMCA [24]. PIGE spectroscopy enables the detection of light elements starting from Li on depending on the energy of incident protons and the nuclear reactions possible [25]. The PIGE sum spectrum of sample AI-HF-03 is presented in Fig. 5a and shows that F, Na, Al and P can be detected in ivory. PIGE maps of these elements are presented in Fig. 5b-e. We selected the ROIs of the different elements corresponding to their peaks

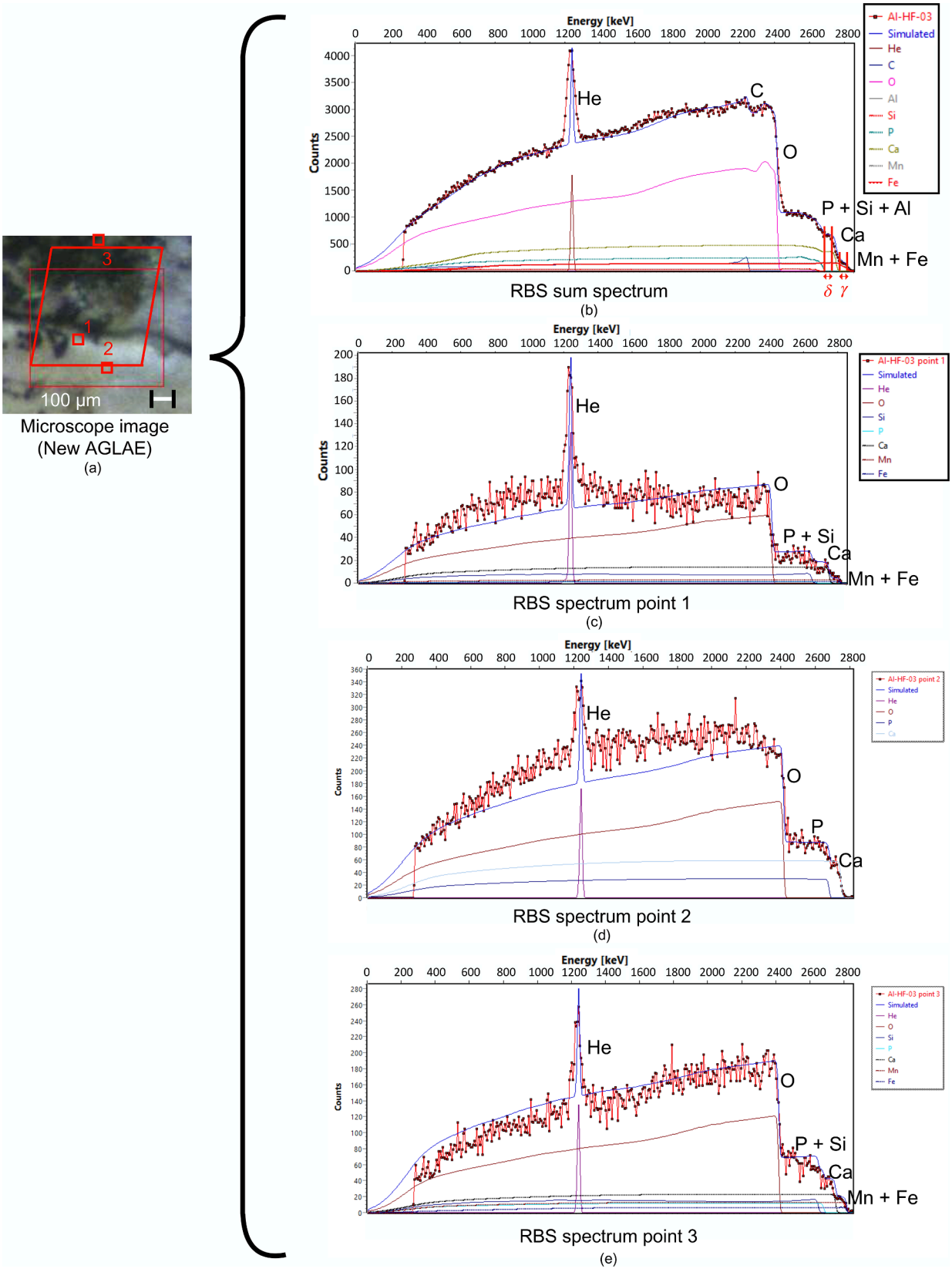


**Fig. 3.** (a) Analyzed area of the cross section of the sample AI-HF-03. An area of 1 mm × 1 mm corresponding approximately to the red parallelogram and three punctual analyses have been carried out. (c) RBS sum spectrum of the whole area. The cross sections are all non-Rutherford except for Al, Ca and P. The analyzed area is the same as for the PIXE mapping. The ROI $\gamma$ has been used to obtain the RBS map of Mn + Fe in the Fig. 7. The RBS map of Ca in the Fig. 7 results from the subtraction of the ROI $\delta$ by the ROI $\gamma$. Both ROIs have an energy width of about 50 keV. (d), (e) and (f) RBS spectra of respectively points 1, 2 and 3.

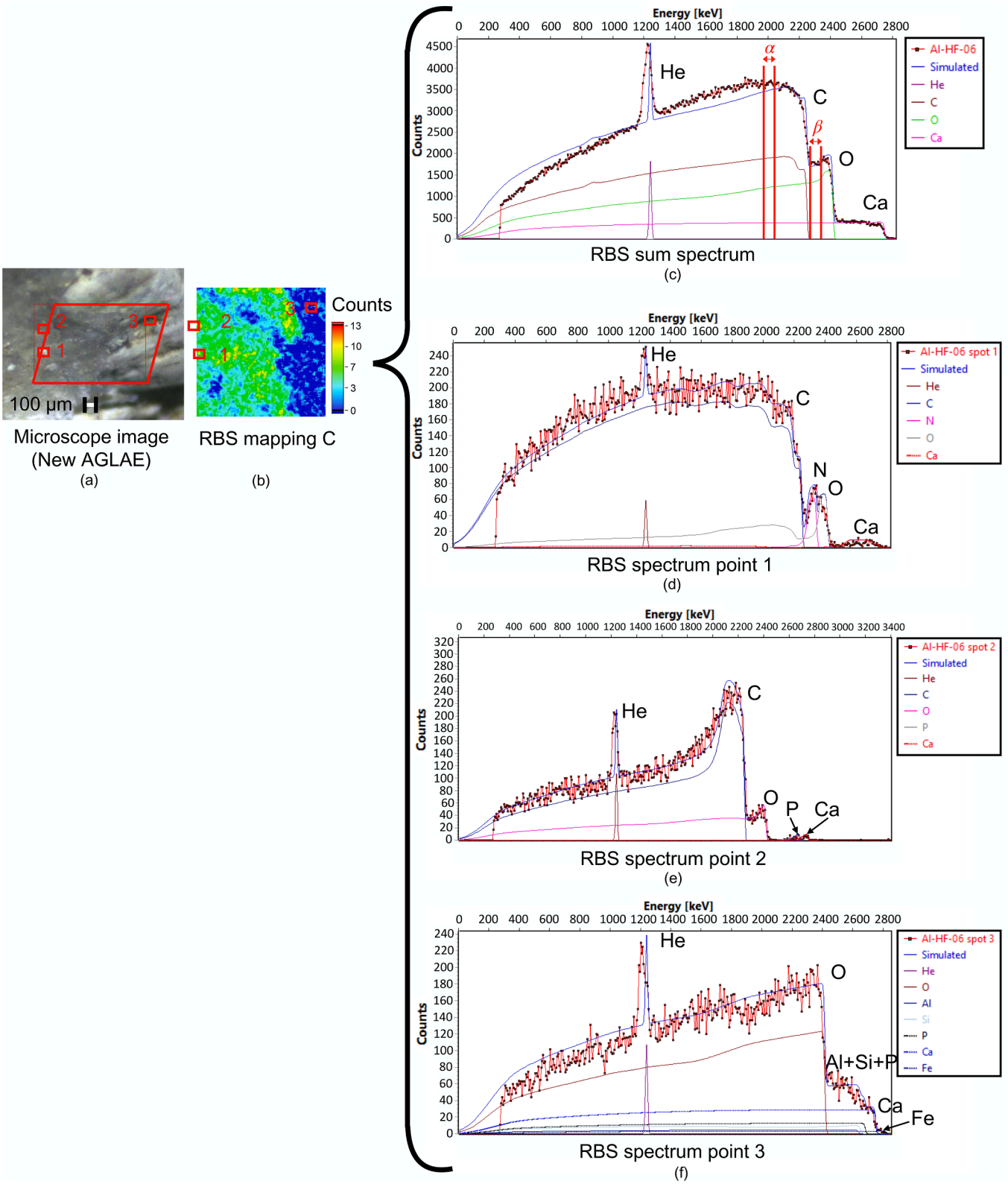


**Fig. 4.** (a) Analyzed area of the cross section of the sample AI-HF-06. An area of 1 mm × 1 mm corresponding approximately to the red parallelogram and three punctual analyses have been carried out. We extracted a map of C (b) from the RBS sum spectrum (c) of the whole area. (d), (e) and (f) RBS spectra of respectively points 1, 2 and 3.

(110 and 197 keV for F, 440 keV for Na, 844 and 1014 keV for Al and 1266 keV for P). For PIGE, in case of two peaks we added the contributions of the two resulting ROIs for the considered element. Then we used a median filter with a width of 3 pixels to mitigate the noise caused by low count rates in the PIGE mappings. For F, the background obtained from the sum spectrum in the ROIs, which corresponds to about 5 counts per pixel, was subtracted. The background for the other elements (less than a count per pixel) was neglected. The PlotAndROI software

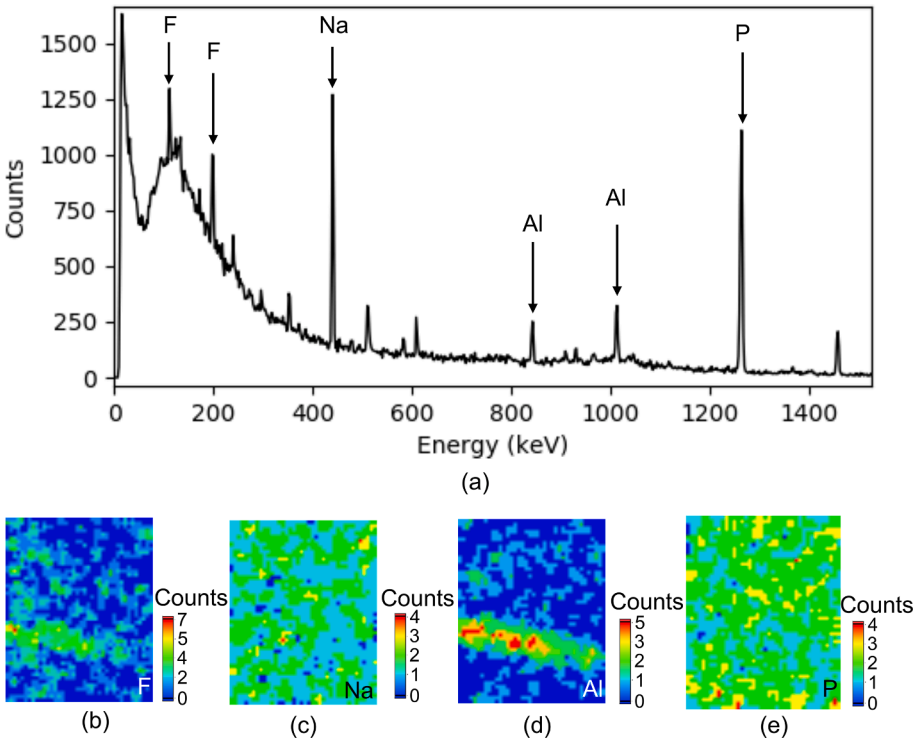


**Fig. 5.** Upper part: (a) PIGE sum spectrum of the sample AI-HF-03. The analyzed area is the same as for the PIXE mapping. Lower part: PIGE maps of the elements F (b), Na (c), Al (d) and P (e) for the sample AI-HF-03 (dimensions: 0.4 mm × 0.5 mm).

(developped by the New AGLAE team) was used to quantify PIGE analysis data based on the analysis of appropriate standards. Quantification of PIXE analysis data were performed using GUPIX and TRAU-PIXE softwares [26,14] and are presented in the SI (Fig. S3 and Table S1).

### 2.4. Differences in elemental sensitivity

The elemental sensitivity differs significantly between the used analytical techniques. There are three main reasons for this difference.

The first reason is related to the set-ups. At the PUMA beamline, the measurements are performed in air, while at New AGLAE the low-energy SDD detector is purged with He. The penetration depth of X-ray emission of light elements ($Z < 15$) does not exceed a few centimeters in air, which roughly corresponds to the distance between the SDD detector and the sample in the PUMA setup ($\geq$3 cm). In contrast, the path length of low-energy X-rays in He atmosphere is on the order of a few meters to hundreds of meters (see Table 1). This is why elements lighter than P cannot be detected at PUMA and is one of the reasons of the higher sensitivity for light elements of PIXE at NewAGLAE.

Second, the interaction cross sections of protons at 3 MeV [27] and photons (photoelectric absorption) at 18 keV [28] behave in opposite ways with increasing energy (see the Fig. S4 in the SI) meaning that protons have a higher probability to interact with light elements and photons with heavier element. The energy of the fluorescence lines of the element Ca around 4 keV represents the threshold between these two tendencies.

Third, another difference between the used methods lies in the information depth. Table 2 shows the calculated values for the information depth of selected elements detected in ivory, the results of which are discussed later in this paper. In PIXE and SR-XRF, the information depth corresponds to the depth from which 95 % of the respective X-ray signal originates. For the main elements of ivory, P and Ca, the information depth is similar between the two methods. For heavier elements (Fe, Zn, Sr and Pb), the emitted X-rays in SR-XRF come from a greater depth than in PIXE. As a result, when considering elements heavier than Fe, PIXE analysis is a more superficial technique than XRF. Moreover, information depth from PIXE tends to quickly stabilize while information depth of XRF continues to increase with the emission of higher energies. In the case of PIGE, the information depth corresponds to the path of protons in ivory until they reach an energy for which the probability of nuclear reactions is low (thick target yield lower than $10^3$ $(\mu C.sr)^{-1}$). This assumption is justified because the absorption of gamma rays is negligible in this material [28,29]. The depth of information that PIGE achieves is relatively high compared to the other techniques, allowing PIGE to examine ivory at greater depth for light elements. To determine the information depth of RBS, the path traveled by the backscattered protons at the lowest energy of the ROI under consideration was calculated. The information depth of RBS lies in the range of a few $\mu$m for characteristic elements in ivory and is even ten times shorter than for PIXE and XRF for transitions metals (Mn, Fe). As a result, RBS has a high surface sensitivity in comparison to the other methods.

**Table 1**
Penetration depth of K-shell X-ray emission of different elements in air and in He gas (the case of He flow in air has not been taken into account). The depth corresponds to 95% of attenuation, computations have been made with GUCSA a subroutine of the GUPIX program [26].

| Elements | Penetration depth in air | Penetration depth in He gas |
|---|---|---|
| | (cm) | (cm) |
| Na | 0.77 | 314 |
| P | 4.8 | 2485 |
| K | 18 | 11051 |
| Ca | 25 | 14735 |
| Fe | 128 | 44204 |

**Table 2**
Information depths of different elements present in ivory depending on the probing technique. Computations have been done with the GUYLS and GUCSA subroutines of the GUPIX program [26] for PIXE, XRF and PIGE information depths. For PIXE and PIGE considered incident particles are 3 MeV protons and for XRF the incident X-rays have an energy of 18 keV. The values are given in μm.

| Elements | Information depth (PIXE) | Information depth (XRF) | Information depth (PIGE) | Information depth (RBS) |
|---|---|---|---|---|
| F | | | 66 | |
| Na | 3.51 | 3.50 | 59 | |
| Al | 8.99 | 8.98 | 52 | 10 |
| Si | 13.7 | 13.7 | | 10 |
| P | 20.1 | 20.4 | 44 | 10 |
| Ca | 50.4 | 64.3 | | 6 |
| Mn | 53.0 | 80.1 | | 5 |
| Fe | 57.1 | 99.1 | | 5 |
| Zn | 65.5 | 211 | | |
| Sr | 68.1 | 633 | | |
| Pb | 68.6 | 478 | | |

## 3. Results

### 3.1. Detection of the organic phase by RBS spectroscopy

Light elements that make up the organic phase of ivory (C, N, and O) can be detected by RBS [23]. This is a major advantage of this method in the study of archaeological ivory, as it provides evidence for the preservation of collagen. However, the detection of light elements, generally heavily affected by diagenetic alteration processes at the surface, is strongly limited by its low information depth of only a few $\mu$m. The study of sample cross sections with fresh surfaces should be privileged, when it is allowed and they are available.

The energy fronts of the backscattered protons observed in RBS spectra depend on the composition of the target material. The heavier an element, the higher the energy of the proton backscattered by this element. Most of the trace elements present in ivory cannot be detected by RBS due to their low concentrations. Therefore, chemical composition information provided by PIXE is used to treat the RBS data.

The RBS results for ivory samples AI-HF-03 and AI-HF-06 are displayed in Figs. 3, 4 and 7. The elements C, O, N, Al, Si, P, Ca, Mn and Fe can be detected in the RBS spectrum of ivory (the He peak is due to the He purging). However, some elements were grouped together (Mn + Fe and Al + Si + P) because their energy fronts are so close together that they cannot be distinguished (limit of RBS energy resolution). In addition, the Al and Si contents in ivory are low compared to P, which means that their RBS signals are likely masked by that of P.

In the case of sample AI-HF-03, almost no C and no N at all were detected (see Fig. 3 containing the RBS sum spectrum and three punctual analyses of AI-HF-03), indicating that the collagen in the analyzed area of this sample was apparently degraded, as is often the case with archaeological ivory [12]. Small amounts of carbon could be from carbonate present in ivory [8]. Collagen might be still preserved on another area of AI-HF-03 or on a cross section if we cut it for example but this discussion is beyond the scope of this article.

In contrast, higher C content was detected for sample AI-HF-06 (Fig. 4c) and RBS mapping of C could be realized (Fig. 4b). Although RBS could energetically resolve it, N was not detected in the sum spectrum. The obtained C map in Fig. 4b shows clearly that the C is heterogeneously distributed over the sample cross section. The area rich in carbon corresponds to the dark grey zone in the microscope image (Fig. 4a). This raises the question of whether N is also present in some areas at higher, detectable concentrations, which would indicate the presence of collagen in these areas. Therefore, three spot analyses with longer acquisition times were performed at suitable positions to improve the signal-to-noise ratio and thus enable the detection of N. Two measurements (points 1 and 2) correspond to the area rich in C. At analysis point 1, both C and N were detected and it can be concluded that collagen is probably still present at this point (Fig. 4d). In contrast, the RBS spectrum of point 2 does not show N (Fig. 4e). It can be assumed that the collagen has been degraded in this zone and that the detected C could originate mainly from carbonates. Finally, the RBS spectrum of point 3 shows neither C nor N (Fig. 4f). This is consistent with its position in the Fig. 4b where the RBS signal of C is the lowest. Only the mineral phase (hydroxyapatite) is detected. These results clearly illustrate the heterogeneity of collagen preservation in ancient ivory.

In addition, 2D mappings for Ca and Mn + Fe were also possible using RBS, but with very low statistics (Fig. 7 in the case of sample AI-HF-03). The results for these elements will be discussed later in the context of the PIXE and SR-XRF mappings providing a more optimized detection of these elements.

### 3.2. Analysis of light elements by PIGE

The PIGE mappings in the Fig. 5 appear relatively noisy due to the low count rates per pixel, close to limit of detection. As shown below, the count rates of PIGE mappings are much lower than for PIXE and SR-XRF mappings due to the lower cross section of gamma-ray reactions (about 0.1 barn) [25] regarding to the cross section of PIXE and SR-XRF interactions (between $10^4$ to $10^2$ barn, see Fig. S4 in the SI) [27,28]. This is why PIXE or SR-XRF mappings yield in much better results (see below), except for F. Nevertheless, information can be read from the 2D maps; while Na and P seem to be homogeneously distributed, Al and F show a heterogeneous distribution pattern.

Fluorine, on the other hand, can only be determined by PIGE - F is an exogenous element that accumulates in the ivory apatite over time and forms stable fluorapatite - F-uptake is a known diagenetic process that is discussed in the context of relative dating. Therefore, the determination of fluorine content is of particular importance for the characterization of ivory. In our study, the F content of the ivory samples was relatively low, but ivory may contain much higher amounts of F up to its nominal value in fluorapatite of 3.8 wt%. In this case, F distribution maps with better statistics could be generated, which can provide information about the F uptake process.

Another important feature of PIGE is its higher depth of information compared to other methods. This means that by means of PIGE, information is obtained from the bulk material deeper in the sample and a larger volume of material is probed. This can avoid sampling only the surface layer for light elements, which is often altered by exchange with the environment. Thus, more reliable quantitative results can be obtained. For this reason, the PIGE results were used to correct the quantification of light elements obtained with PIXE (see section 2.3 Data evaluation and mapping representation mode).

### 3.3. Complementarity of IBA and SR-XRF imaging

Fig. 6 shows the PIXE and SR-XRF sum spectra of mappings performed on ivory sample AI-HF-03. By comparing the signal to background ratios, differences in the sensitivity can be deduced between low and high energy detectors for PIXE and SR-XRF. PIXE is well suitable for the detection of lighter elements in ivory such as Al, Si and P (Fig. 6a) as well as of transition elements such as Fe and Zn (Fig. 6b). However, heavier elements can be poorly detected under the given measurement conditions. Fig. 6c refers to the SR-XRF sum spectrum. All elements present in ivory with fluorescence emissions between 3 keV and 16 keV (from P to Pb) can be detected with relatively high sensitivity.

The PIXE and SR-XRF maps of selected elements obtained for sample AI-HF-03 are displayed in Fig. 7 or in the Figs. S1–S3 in the SI. Maps of the major elements of the mineral phase of ivory, P and Ca, are comparable for both methods, even though the obtained count rates differ from each other. The distribution maps of these elements show homogeneous distribution over the scanned area, except in the crack, which is consistent with their endogenous nature. Zinc and Sr are endogenous trace elements that also display a homogeneous distribution except in

the crack. SR-XRF and PIXE maps of exogenous minor (Al, Si) and trace (Fe, Pb) elements show similar distribution patterns. All these elements are mainly localized in the crack, which is a typical signature of elements accumulated in ivory by diagenetic processes.

On the one hand, elemental distribution maps for light elements such as Al and Si can be obtained with PIXE at New AGLAE, which is not possible by means of SR-XRF at the PUMA beamline.

On the other hand, SR-XRF 2D maps show higher count rates for transition and heavier elements ($Z \geq 26$ (Fe)) compared to PIXE, resulting in better statistics and improved detection limits as also shown in Tranchant *et al.* [11]. The limit of detection at PUMA depends on the element but varies also from a few hundreds to a few tens of ppm [13]. Thus, mapping of Pb was possible by means of SR-XRF, which is present in the studied ivory samples at very low concentrations (<0.01 wt% [11]), with promising results.

The spatial resolution of SR-XRF images is determined by the size of the beam and the step size, which are approximately equal (10 μm). The size of the proton beam (about 40 μm × 40 μm) is larger than the selected step size (10 μm). This induces a blurring of the PIXE mappings regarding to the XRF mappings due to an oversampling during the measurement.

In particular, better image qualities are obtained for the transition metals such as Fe and Zn using SR-XRF, justified by the higher statistics together with the higher spatial resolution.

These measurement results illustrate the complementarity of these two imaging techniques.

### 3.4. Additional information by RBS imaging

RBS maps of sample AI-HF-03 could be obtained for Ca and Mn + Fe and are given in the Fig. 7. They show very low statistics in comparison to the ones of PIXE and of SR-XRF because the ROI to extract the RBS signal concerning only Ca or Mn + Fe has a very small energy width (see Fig. 3b) due to the relatively low backscattering cross-sections with respect to the interaction cross sections of protons and photons (data extracted from the IBANDL data base http://www-nds.iaea.org/ibandl/).

The Ca distribution maps are comparable between the three methods (see Fig. S7 in the SI), although the depth of information is very different. In contrast, the RBS map of Mn + Fe shows an interesting deviation. The high concentration of Mn and Fe in the crack, which is the most characteristic feature of the PIXE/XRF mappings (Figs. 7 and S1–S3 in the SI), is not present in the RBS map. (It can be ruled out that this absence is due to a shift in frontal energy caused by an additional air layer but is more probably related to geometrical effects, as explained in detail in the SI, see Figs. S6–S8). RBS is obviously highly sensitive to the morphology of the sample due to its low information depth, and thus the material deposited in the crack cannot be detected. In contrast, the RBS map shows an area of high Mn and Fe content in the upper left part, which is also evident in the PIXE/XRF mappings. In this area, the sample has a smooth surface. From the depth of information of the RBS for Mn and Fe, it can be inferred that Mn and/or Fe are present at this location in the uppermost surface layer (within 5 μm). This additional information could not be derived from the PIXE or SR-XRF mappings and confirms the exogenous character of Mn and Fe in the ivory.

## 4. Conclusions and outlook

The presented analytical approach based on a combination of complementary analytical methods was developed in order to non-invasively characterize ancient ivory artefacts as complete as possible taking into account the heterogeneity of the material. As an overall aim of this study, this analytical approach intends to help getting new insights into the archaeological context of prehistoric mammoth ivory

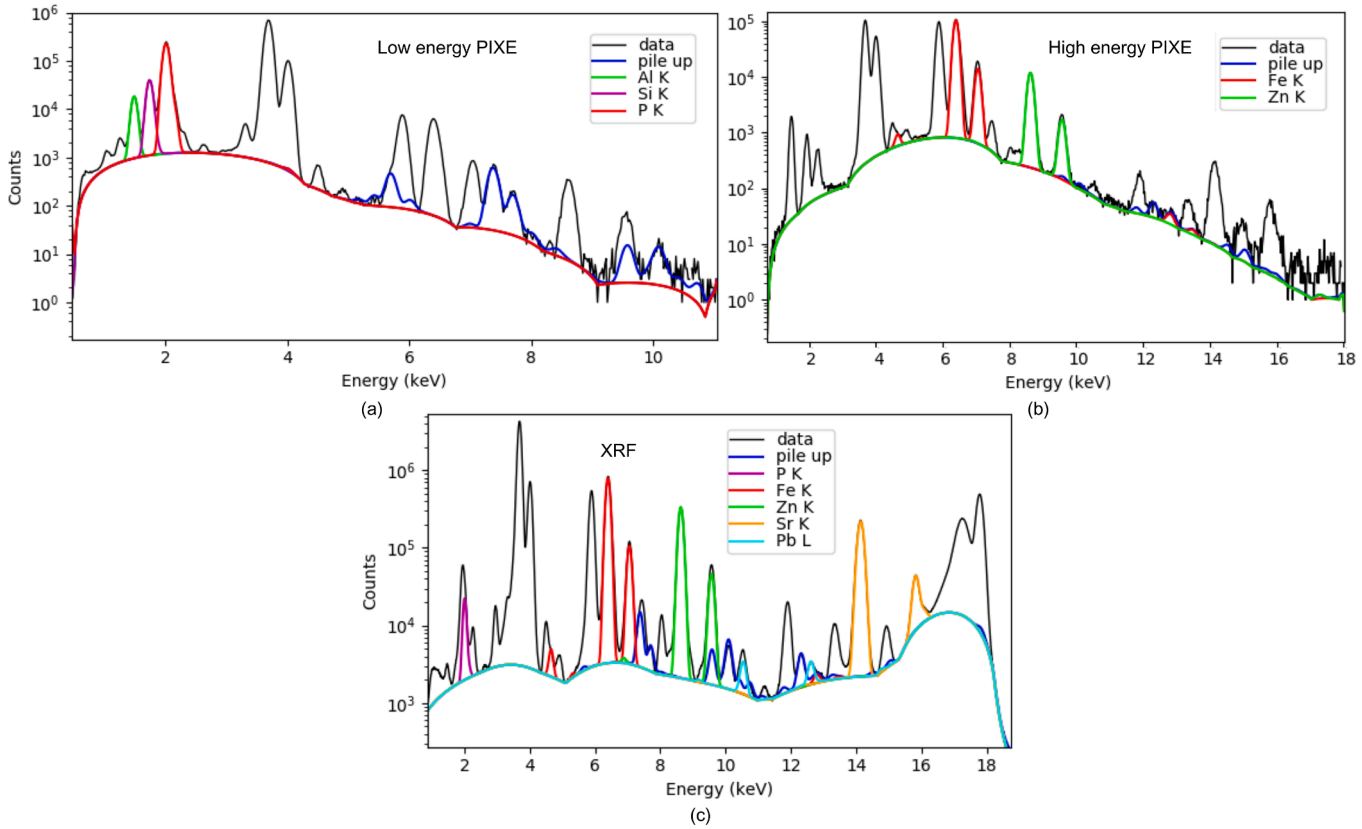


**Fig. 6.** PIXE sum spectra of the sample AI-HF-03 respectively for the low energy detector (a) and the high energy detector (b) and XRF sum spectrum (c). In each spectrum we present the fits of the elements whose mappings are shown in Fig. 7.

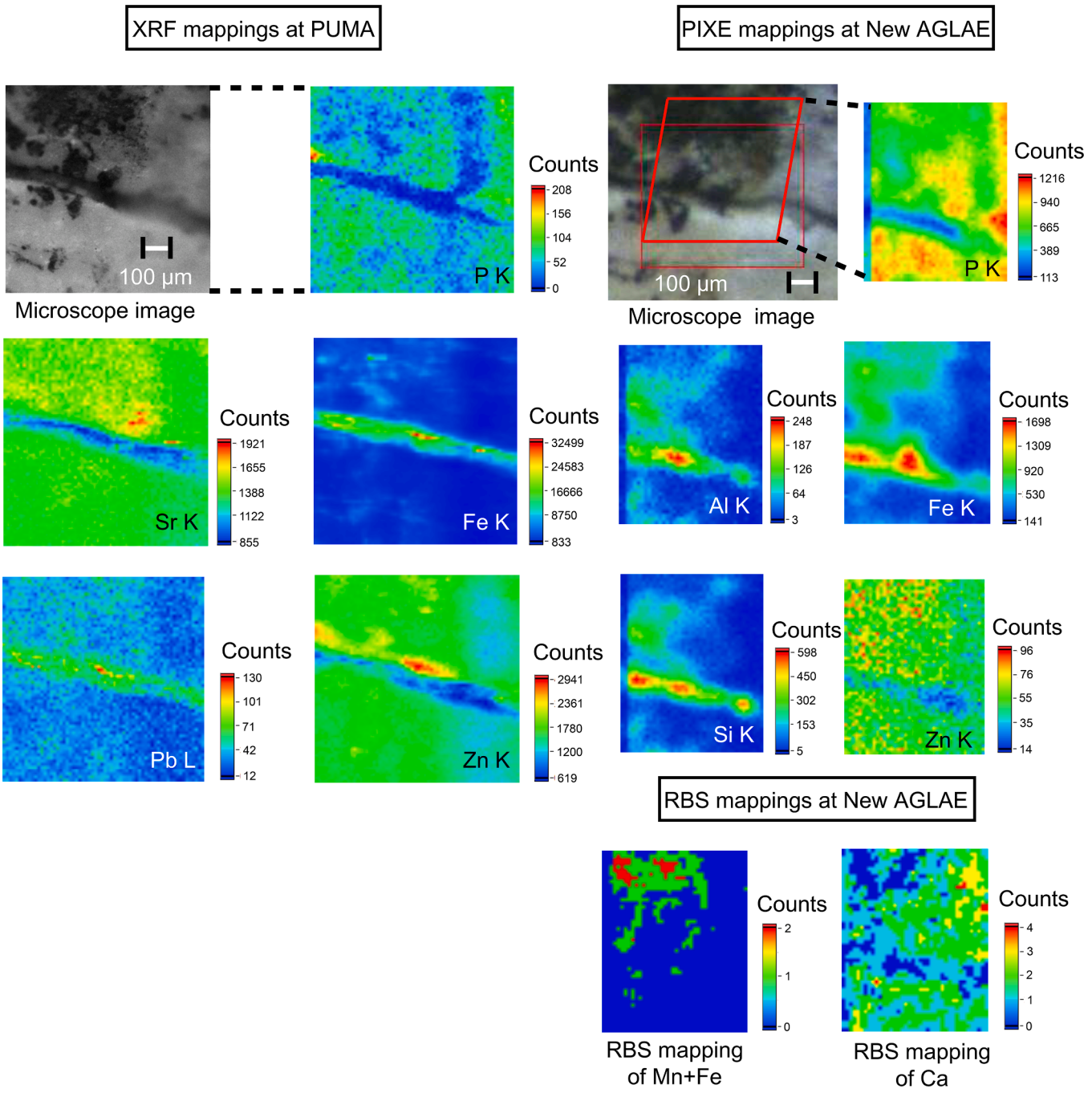


**Fig. 7.** Comparison of SR-XRF, PIXE and RBS mappings of the sample AI-HF-03. The red rectangle on the microscope image at NewAGLAE shows the supposed analyzed area (approximately 0.4 × 0.5 $mm^2$) for PIXE and RBS mappings. However, the analysed area tends to look like the parallelogram added in red. The distorsion comes from the difficulties to align the beam and the microscope for a non flat area and that the microscope is not in the same plan as the beam.

artifacts and their state of preservation. This paper highlights the complementarity of IBA methods and SR-XRF in this respect. PIXE/PIGE/RBS at the New AGLAE facility allows detection of all elements from C to U with satisfactory detection limits. The strength of the set-up lies in the detection of light elements ($Z \leq 20$) allowing the characterization of the organic matrix of ivory (collagen), when it is sufficiently preserved at the surface by means of RBS. In combination with IBA, SR-XRF at the PUMA beamline is in particular appropriate to detect heavier elements especially for $Z \geq 20$ even if detection is possible from $Z \geq 11$ on, but with significant lower signal intensities. SR-XRF provides higher sensitivity and allow the detection of heavier trace elements (e.g. Cu, Pb) better than PIXE.

The differences in information depth of the applied methods could be used to obtain some kind of depth-resolved information. PIGE provides a higher depth of information, which corresponds more to bulk analyses and is therefore less influenced by the changed surface composition. Thus, it contributes to a more accurate quantification of the composition of old ivory, especially for light elements ($Z \leq 20$). At New AGLAE, methodological improvements for light elements are currently in progress which will improve the PIGE performances. For heavier elements ($Z \geq 20$), PIXE is more surface sensitive than SR-XRF. Therefore, SR-XRF represents a better bulk analysis than PIXE. RBS is the most surface sensitive among the applied methods with an information depth of a few $\mu$m to a maximum of about 35 µm for ivory considering the path

travelled by the detected backscattered protons forming the RBS spectrum (from 3 MeV to less than 200 keV). The enhanced information depth of PIGE with respect to RBS and PIXE could also be used as a method for characterizing radiation-induced changes in the ivory material, a topic of current research in the field of heritage science. Indeed, the fact that radiation-induced changes can occur in ancient materials for methods such as IBA and synchrotron-based techniques is now recognized and safe boundaries of analyses need to be defined [30].

The imaging tools at both facilities allow revealing the elemental distributions from C to U with high spatial resolution. The acquired maps give hints on the endo- or exogeneous character of certain elements in ancient ivory, whose composition is generally altered with respect to modern elephant or well preserved permafrost mammoth ivory references. They thus allow drawing conclusions on taphonomical processes leading to e.g. local preservation of collagen. Such information is crucial for selecting and optimizing dedicated samples in the ivory artefacts for further isotopic analyses used for the determination of diets, provenancing or dating that are of important archaeological relevance.

## CRediT authorship contribution statement

**L. Tranchant:** Software, Validation, Formal analysis, Investigation, Data curation, Writing – original draft, Visualization. **K. Müller:** Conceptualization, Methodology, Validation, Formal analysis, Investigation, Data curation, Writing – review & editing, Visualization, Supervision. **Q. Lemasson:** Software, Validation, Formal analysis, Investigation, Data curation. **L. Pichon:** Software, Validation, Formal analysis, Investigation, Data curation. **S. Schöder:** Methodology, Software, Validation, Formal analysis, Investigation, Resources, Data curation, Writing – review & editing, Supervision, Funding acquisition. **N.J. Conard:** Resources, Project administration, Funding acquisition. **I. Reiche:** Conceptualization, Methodology, Validation, Formal analysis, Investigation, Resources, Data curation, Writing – review & editing, Visualization, Supervision, Project administration, Funding acquisition.

## Declaration of Competing Interest

The authors declare the following financial interests/personal relationships which may be considered as potential competing interests: Ina Reiche reports administrative support was provided by National Graduate School of ChemistryParis. Ina Reiche reports financial support was provided by IPERION CH European Infrastructure. Quentin Lemasson, Laurent Pichon reports financial support was provided by CNRS Paris B Delegation, ANR − 10 EQPX 22 New AGLAE.

## Data availability

Data will be made available on request.

## Acknowledgements

We thank the many members of the excavation and laboratory teams at Hohle Fels, without whose hard work this study would be impossible. We thank also Angélique Rouquié for the technical support on the PUMA beamline. We acknowledge the measurement time allowance by the synchrotron SOLEIL at the PUMA beamline through the proposal number 20200168. The ion beam analysis experiments were performed at the New AGLAE facility (ANR - 10 EQPX 22). We thank Brice Moignard, Jean-Paul Berthet and Claire Pacheco, the other members of the New AGLAE team.

*Funding*

This work was supported by the German Research Foundation (DFG), the Ministry for Science, Research and Art (MWK) of Baden-Württemberg, the ROCEEH project of the Heidelberg Academy of Sciences and the Eberhard Karls Universität Tübingen for the excavation and research at Hohle Fels; the french National Research Agency (ANR) EquipEx project [grant number ANR10-EQPX-22]; the European infrastructure program IPERION CH [Grant agreement no. 654028].

## Appendix A. Supplementary data

Supplementary data to this article can be found online at https://doi.org/10.1016/j.nimb.2023.165146.

## References

[1] J. Lee-Thorp, M. Sponheimer, Contributions of biogeochemistry to understanding hominin dietary ecology, Am. J. Phys. Anthropol. 131 (S43) (2006) 131–148.
[2] L. Rey, T. Tacail, F. Santos, S. Rottier, G. Goude, V. Balter, Disentangling diagenetic and biogenic trace elements and sr radiogenic isotopes in fossil dental enamel using laser ablation analysis, Chem. Geol. 587 (2022), 120608.
[3] N.J. Conard, Palaeolithic ivory sculptures from southwestern germany and the origins of figurative art, Nature 426 (6968) (2003) 830–832.
[4] S. Wolf, C. Heckel, Ivory ornaments of the aurignacian in western europe: case studies from france and germany, L'anthropologie 122 (3) (2018) 348–373.
[5] F. Cui, H. Wen, H. Zhang, C. Ma, H. Li, Nanophase hydroxyapatite-like crystallites in natural ivory, J. Mater. Sci. Lett. 13 (14) (1994) 1042–1044.
[6] K. Müller, I. Reiche, Differentiation of archaeological ivory and bone materials by micro-PIXE/PIGE with emphasis on two Upper Palaeolithic key sites: Abri Pataud and Isturitz, France, J. Archaeolog. Sci. 38 (12) (2011) 3234–3243.
[7] I. Reiche, C. Heckel, K. Müller, O. Jöris, T. Matthies, N.J. Conard, H. Floss, R. White, Combined non-invasive pixe/pige analyses of mammoth ivory from aurignacian archaeological sites, Angew. Chem. Int. Ed. 57 (25) (2018) 7428–7432.
[8] I. Reiche, L. Favre-Quattropani, T. Calligaro, J. Salomon, H. Bocherens, L. Charlet, M. Menu, Trace element composition of archaeological bones and post-mortem alteration in the burial environment, Nucl. Instrum. Methods Phys. Res., Sect. B 150 (1–4) (1999) 656–662.
[9] C. Heckel, K. Müller, R. White, S. Wolf, N.J. Conard, C. Normand, H. Floss, I. Reiche, F-content variation in mammoth ivory from aurignacian contexts: Preservation, alteration, and implications for ivory-procurement strategies, Quat. Int. 403 (2016) 40–50.
[10] M. Albéric, K. Müller, L. Pichon, Q. Lemasson, B. Moignard, C. Pacheco, E. Fontan, I. Reiche, Non-invasive quantitative micro-pixe–rbs/ebs/ebs imaging reveals the lost polychromy and gilding of the neo-assyrian ivories from the louvre collection, Talanta 137 (2015) 100–108.
[11] L. Tranchant, K. Müller, Q. Lemasson, L. Pichon, S. Schöder, N. Conard, I. Reiche, Improved discrimination of biogenic and diagenetic elements in palaeolithic mammoth ivory and bone from Hohle Fels cave in the swabian jura of southwestern germany, Quaternary International https://doi.org/10.1016/j.quaint.2023.02.006. URL https://www.sciencedirect.com/science/article/pii/S1040618223000368.
[12] L. Beck, J.-P. Cuif, L. Pichon, S. Vaubaillon, A.D. Malassé, R. Abel, Checking collagen preservation in archaeological bone by non-destructive studies (micro-ct and iba), Nucl. Instrum. Methods Phys. Res., Sect. B 273 (2012) 203–207.
[13] P. Tack, B. Bazi, B. Vekemans, T. Okbinoglu, F. Van Maldeghem, S. Goderis, S. Schöder, L. Vincze, Investigation of (micro-) meteoritic materials at the new hard x-ray imaging puma beamline for heritage sciences, J. Synchrotron Radiat. 26 (6) (2019) 2033–2039.
[14] L. Pichon, T. Calligaro, Q. Lemasson, B. Moignard, C. Pacheco, Programs for visualization, handling and quantification of PIXE maps at the AGLAE facility, Nucl. Instrum. Methods Phys. Res., Sect. B 363 (2015) 48–54.
[15] M. Cotte, A. Genty-Vincent, K. Janssens, J. Susini, Applications of synchrotron x-ray nano-probes in the field of cultural heritage, C. R. Phys. 19 (7) (2018) 575–588.
[16] C. Heckel, K. Müller, R. White, H. Floss, N. Conard, I. Reiche, Micropixe/pige analysis of palaeolithic mammoth ivory: Potential chemical markers of provenance and relative dating, Palaeogeogr. Palaeoclimatol. Palaeoecol. 416 (2014) 133–141.
[17] N.J. Conard, M. Malina, S.C. Münzel, New flutes document the earliest musical tradition in southwestern germany, Nature 460 (7256) (2009) 737–740.
[18] L. Pichon, L. Beck, P. Walter, B. Moignard, T.h. Guillou, A new mapping acquisition and processing system for simultaneous PIXE-RBS analysis with external beam, Nucl. Instrum. Methods Phys. Res., Sect. B 268 (11–12) (2010) 2028–2033.
[19] J. Salomon, J.-C. Dran, T. Guillou, B. Moignard, L. Pichon, P. Walter, F. Mathis, Present and future role of ion beam analysis in the study of cultural heritage materials: The example of the AGLAE facility, Nucl. Instrum. Methods Phys. Res., Sect. B 266 (10) (2008) 2273–2278, https://doi.org/10.1016/j.nimb.2008.03.076. https://doi.org/10.1016%2Fj.nimb.2008.03.076.
[20] T. Calligaro, Y. Coquinot, L. Pichon, B. Moignard, Advances in elemental imaging of rocks using the aglae external microbeam, Nucl. Instrum. Methods Phys. Res., Sect. B 269 (20) (2011) 2364–2372.
[21] A. Thompson, et al., X-ray data booklet (center for x-ray optics and advanced light source, lawrence berkeley national laboratory, berkeley, ca, 2009).
[22] M. Mayer, Simnra user's guide.
[23] L. Beck, L. Pichon, B. Moignard, T. Guillou, P. Walter, Iba techniques: Examples of useful combinations for the characterisation of cultural heritage materials, Nucl. Instrum. Methods Phys. Res., Sect. B 269 (24) (2011) 2999–3005.

[24] V. Solé, E. Papillon, M. Cotte, P. Walter, J. Susini, A multiplatform code for the analysis of energy-dispersive x-ray fluorescence spectra, Spectrochim. Acta B At. Spectrosc. 62 (1) (2007) 63–68.
[25] Development of a Reference Database for Particle Induced Gamma Ray Emission (PIGE) Spectroscopy, no. 1822 in TECDOC Series, INTERNATIONAL ATOMIC ENERGY AGENCY, Vienna, 2017. URL https://www.iaea.org/publications/12235/development-of-areference-database-for-particle-induced-gamma-ray-emissionpige-spectroscopy.
[26] J.L. Campbell, T.L. Hopman, J.A. Maxwell, Z. Nejedly, The guelph pixe software package iii: alternative proton database, Nucl. Instrum. Methods Phys. Res., Sect. B 170 (1–2) (2000) 193–204.
[27] Y. Wang, M.A. Nastasi, Handbook of modern ion beam materials analysis, Materials Research Society Pittsburgh, PA, 2009.
[28] M. Berger, J. Hubbell, S. Seltzer, J. Chang, J. Coursey, R. Sukumar, D. Zucker, K. Olsen, Xcom: Photon cross sections database, nist standard reference database 8 (xgam), URL http://physics.nist. gov/PhysRefData/Xcom/Text/XCOM.html.
[29] A. Subercaze, Utilisation combinée des rayons x et gamma émis lors de l'interaction avec la matière d'ions légers aux énergies intermédiaires: des mécanismes primaires de réaction aux applications, Ph.D. thesis, Ecole nationale supérieure Mines-Télécom Atlantique Bretagne Pays de la Loire (2017).
[30] L. Bertrand, S. Schöder, D. Anglos, M.B.H. Breese, K. Janssens, M. Moini, A. Simon, Mitigation strategies for radiation damage in the analysis of ancient materials, TrAC Trends Anal. Chem. 66 (2015) 128–145, https://doi.org/10.1016/j.trac.2014.10.005.